Impact of Spatial Correlation on Adaptive Coded Modulation Performance in Rayleigh Fading

Bengt Holter and Geir E. Øien

***Abstract*— A performance analysis of an adaptive coded modulation (ACM) scheme operating on identically distributed and spatially correlated Rayleigh flat-fading channels is presented. In particular, a single-input multiple-output system using maximum ratio combining at the receiver is considered. The ACM scheme consists of a set of multidimensional trellis codes originally designed for additive white Gaussian noise channels, with codes being based on quadrature amplitude modulation signal constellations of varying size. Rate adaptation is achieved by providing the transmitter with channel state information as predicted by the receiver. Numerical examples are given for the case of Jakes correlation profile and *maximum a posteriori*-optimal predictor coefficients, and results are compared to previously published results for spatially uncorrelated channels.**

***Index Terms*— Adaptive coded modulation, spatial correlation, fading channels, diversity.**

I. INTRODUCTION

Adaptive coded modulation (ACM) is a promising tool for increasing the spectral efficiency of time-varying mobile channels while maintaining a predictable bit error rate (BER) [1]–[5]. The concept of ACM is to transmit with high information rates under favorable channel conditions and to reduce the information rate in response to channel degradation. An important restriction is that the transmitter needs to have accurate channel state information (CSI), which in many applications must be estimated by the receiver and conveyed to the transmitter on a dedicated feedback channel.

Naturally, a time delay is associated with transmission of data on the feedback channel. Due to channel fluctuations during this time delay, the reported CSI may deviate from the true state of the channel by the time it is used by the transmitter. To alleviate this problem, a CSI predicted *ahead in time* may be reported, rather than reporting the instantaneous CSI. In [6], the effects of such a method are investigated by describing how estimation error and feedback delay affect some key performance measures of an ACM system when using a linear fading-envelope predictor on each individual branch of a maximum ratio combining (MRC) receiver. An important part of this analysis is based on the knowledge of the joint distribution of the true and predicted *channel signal-to-noise ratio* (CSNR) at the output of the MRC receiver, since the correlation between these two entities is an important parameter affecting the error performance. In [6], the MRC receiver is assumed to be operating on spatially independent and identically distributed Rayleigh flat-fading channels and as such, the joint distribution of the true and the predicted CSNR can be represented by a bivariate gamma distribution, since they both are individually gamma distributed and mutually correlated.

B. Holter is with SINTEF ICT, Communication Systems, Trondheim, Norway (e-mail: bengt.holter@sintef.no) G. E. Øien is with the Norwegian University of Science and Technology, Signal Processing Group, Trondheim, Norway (e-mail: geir.oien@iet.ntnu.no)

In this paper, the results in [6] are extended to include identically distributed but spatially *correlated* Rayleigh flat-fading channels. However, as in [6], both channel estimation and prediction are performed independently on each branch. Hence, from a prediction perspective, the advantage of spatial correlation between the branches of the MRC receiver is not exploited. The reason for this is that we in this paper aim primarily to quantify the performance degradation of the ACM scheme in [6] when the design assumption of spatially uncorrelated channels is incorrect. In other words, the system is assumed to have been explicitly designed for spatially uncorrelated channels, but operates on spatially correlated channels, and the analysis in the paper documents the consequences of this mismatch. A performance improvement achieved by exploiting a more advanced predictor taking spatial correlation into account is a topic for further research.

In the presence of spatial correlation, neither the true nor the predicted CSNR at the output of the MRC receiver will be gamma distributed. However, the same type of analysis as in [6] may be pursued with good accuracy if the densities of both the true and the predicted CSNR are *approximated* by gamma distributions. To this end, an approximate probability density function (PDF) of the combined CSNR in MRC systems operating on correlated Nakagami-m fading channels is utilized [7]. In particular, results for Rayleigh fading channels are presented by letting the Nakagami-m parameter be equal to 1 $(m = 1)$.

II. SYSTEM AND CHANNEL MODEL

The rate-adaptive system depicted in Figure 1 is considered. Channel estimation is based on periodic insertion of pilot symbols which can be viewed as sampling of a band-limited process. Denoting the transmitted complex baseband signal (after pilot-symbol insertion) at time index i by $x(i)$, the received signal on branch b at time index i can be written as $y_b(i) = z_b(i) \cdot x(i) + n_b(i)$, where $z_b(i)$ and $n_b(i)$ are the complex fading amplitude and the additive white Gaussian noise (AWGN) component, respectively. The signal $x(i)$ contains information except at the pilot symbol instants. As in [6], it is assumed that all pilot symbols have the same absolute value and that data and pilot symbols are transmitted with the same power. The transmission rate is adapted using a set of N

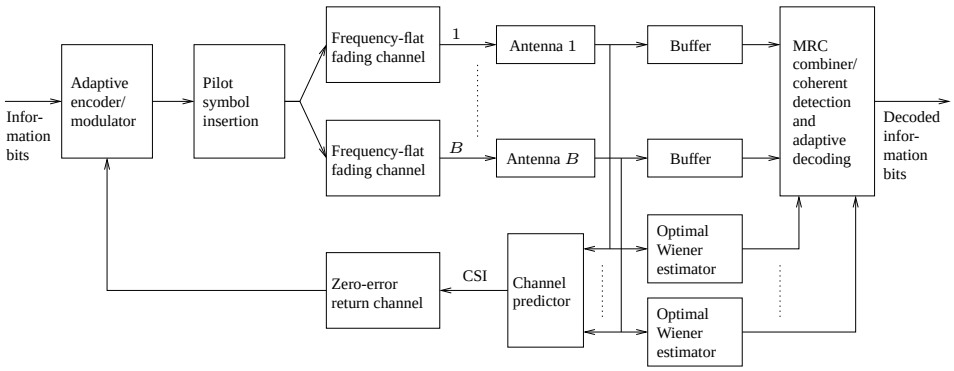


Fig. 1. ACM system with pilot-symbol-assisted channel estimation (for coherent detection purposes) and prediction (for transmitter adaptation purposes).

multidimensional trellis codes originally designed for AWGN channels [4]. The codes are based on quadrature amplitude modulation (QAM) signal constellations and rate adaptation is performed by splitting the received CSNR range into $N+1$ fading regions (bins). Each bin is associated with one code n. The lower thresholds of each bin, $\{\gamma_n\}_{n=1}^{N}$, are selected such that a target BER—denoted BER_0—is always achieved for each available code in the rate-adaptive scheme, provided the code is chosen based on perfect CSNR knowledge. When the CSNR at the output of the MRC receiver, γ, falls within fading region n ($\gamma_n \leq \gamma < \gamma_{n+1}$), the associated CSI, i.e. the fading region index n, is sent back to the transmitter. The transmitter then adapts its transmission rate and coding scheme according to the quality of the channel by transmitting with a code realizing a spectral efficiency of R_n. If $0 \leq \gamma < \gamma_1$, transmission of information symbols is temporarily suspended (outage), and information must be buffered at the transmitter end.

To alleviate the outdated CSI problem, the receiver reports a *predicted* CSI ahead in time rather than reporting the instantaneous CSI. The CSNR on each branch is predicted every time a new pilot symbol arrives, and a computationally intensive predictor, optimal in the *maximum a posteriori* (MAP) sense, is used. The prediction is based on channel estimates from an optimal noncausal Wiener interpolator filter. This filter will smooth the noise and improve reliability beyond what can be achieved by a predictor. It can then be assumed that the estimation error in the receiver is negligible compared to the prediction error, i.e. true coherent detection can be assumed. Each channel is assumed to be slowly varying so that the fading remains relatively constant over many channel symbols

By assumption, the fading amplitude $|z_b(i)| \triangleq \alpha_b$ is a Rayleigh distributed random variable (RV). The instantaneous fading power, α_b^2, may then be viewed as a gamma distributed RV with shape factor 1 and scale factor Ω, where $\Omega = \mathcal{E}\{\alpha_b^2\}$ is the average fading power of the channel.[1] It follows by transformation of random variables that the associated CSNR on branch b, $\gamma_b = \frac{\alpha_b^2 P}{N_0 W}$, is a gamma distributed RV with mean $\overline{\gamma}_b = \frac{\Omega P}{N_0 W}$, where P [W] is the constant average transmit power, N_0 [W/Hz] is the one-sided power spectral density of the complex AWGN on each channel, and W [Hz] is the one-sided information bandwidth. Due to our assumption of identically distributed channels, both Ω and $\overline{\gamma}_b$ will be independent of b. However, the latter will be indexed by b anyway, to indicate that this is the average CSNR per branch and not the average *combined* CSNR at the output of the MRC receiver.

III. Statistics of the combined CSNR

For an MRC receiver with B branches, the combined CSNR γ may be expressed as $\gamma = \sum_{b=1}^{B} \gamma_b$, where $\gamma \sim \mathcal{G}(B, \overline{\gamma}_b)$ in case of uncorrelated branches. Linear channel prediction[2] is performed independently on each branch, and the prediction of the combined CSNR (ahead in time) is given by [6] $\hat{\gamma} = \sum_{b=1}^{B} \hat{\gamma}_b$, where $\hat{\gamma}_b = \frac{\hat{\alpha}_b^2 P}{N_0 W}$ is the predicted CSNR on branch b, and $\hat{\alpha}_b^2$ is the predicted fading power on branch b. For uncorrelated antennas, $\hat{\gamma}$ is distributed according to $\hat{\gamma} \sim \mathcal{G}(B, r\overline{\gamma}_b)$, where r is a constant which depends on the predictor coefficients [6]. The joint distribution of γ and $\hat{\gamma}$ is then a bivariate gamma distribution, because γ and $\hat{\gamma}$ both are individually gamma distributed and mutually correlated [6].

In the presence of spatial correlation however, both γ and $\hat{\gamma}$ represent sums of correlated gamma variates, so the joint distribution needed to quantify the correlation ρ between γ and $\hat{\gamma}$ is not known. However, according to [7], the exact PDF of a sum of correlated gamma variates may be *approximated* by a gamma distribution with the first two moments identical to those of the exact distribution. As a result, both γ and $\hat{\gamma}$ are in this paper viewed as gamma distributed RVs and distributed according to $\gamma \sim \mathcal{G}(\psi, \theta)$ and $\hat{\gamma} \sim \mathcal{G}(\psi, r\theta)$, where the shape and scale factors ψ and θ needed to generate the correct moments in question are listed in Table I. The results are derived from [8] and are valid for a system operating on identically distributed and spatially correlated Nakagami-m fading channels, where ρ_s is the normalized spatial power

[1] X follows a gamma distribution with shape factor $\psi > 0$ and scale factor $\theta > 0$ when the PDF of X is given by $f_X(x) = \frac{x^{\psi-1} e^{-x/\theta}}{\theta^{\psi}\Gamma(\psi)} U(x)$, where $\Gamma(\cdot)$ is the gamma function and $U(\cdot)$ is the unit step function. The short hand notation $X \sim \mathcal{G}(\psi, \theta)$ is used to denote that X follows a gamma distribution with shape factor ψ and scale factor θ. With this definition of the gamma distribution, the mean $\overline{x} = \mathcal{E}\{X\} = \psi\theta$ and the variance $\sigma_X^2 = \mathcal{E}\{X^2\} - \overline{x}^2 = \psi\theta^2$. $\mathcal{E}\{\cdot\}$ denotes the statistical average.

[2] The channel prediction procedure employed in this paper is identical to the one presented in [6], so the interested reader is referred to [6] for further details to avoid repetitive comments.

correlation coefficient between two adjacent antennas. The joint PDF of γ and $\hat{\gamma}$ can then be represented by a bivariate gamma distribution, i.e. $\gamma, \hat{\gamma} \sim \mathcal{G}(\psi, \theta, r\theta, \rho)$ [6].

In [9], it is demonstrated that in terms of average spectral efficiency (ASE) [bit/s/Hz] and average BER, the introduced approximation is applicable and valid with good accuracy for $B = 2$ when $0 \leq \overline{\gamma}_b \leq 40$ dB, and for $B = 4$ when $0 \leq \overline{\gamma}_b \leq 30$ dB. The reason for introducing an upper bound on $\overline{\gamma}_b$ is that the approximate PDF does not contribute to realize the true slope (diversity order) or coding gain of the error rate curve at high CSNR. In the next section, this fact is demonstrated by relating some recent results by Wang and Giannakis [10] to a fixed rate single-input multiple-output (SIMO) system using an MRC receiver.

IV. Diversity order and coding gain

In [10], the average symbol error rate (SER)—denoted P_E—of an uncoded (or coded) system at high CSNR is approximated by the expression $P_E \approx (G_c \cdot \overline{\gamma})^{-G_d}$, where G_c represents the coding gain, G_d represents the diversity order, and $\overline{\gamma}$ is the received average CSNR. The diversity order determines the slope of the error rate curve versus $\overline{\gamma}$ at high CSNR in a log-log scale, whereas the coding gain (in dB) determines the shift of this curve in CSNR relative to a benchmark curve given by $(\overline{\gamma}^{-G_d})$.

The intuition behind the approach in [10] is that when the average CSNR is high, the error rate performance will be dominated by the low-probability event that the instantaneous CSNR becomes small. Hence, the behavior of the *lower tail* of a PDF will determine the error rate performance at high CSNR. To analytically quantify this difference and its impact on the error rate performance at high CSNR, expressions for G_c and G_d are presented for a fixed rate SIMO system using an MRC receiver. In particular, results are obtained for identically distributed and spatially correlated Nakagami-m fading channels, in which case the exact PDF is equal to [11, Eq. (5)], and the approximate PDF is a gamma distribution, i.e. $\gamma \sim \mathcal{G}(\psi, \theta)$.

Based on the exact PDF in [11, Eq. (5)], the moment generating function (MGF) of the CSNR at the output of an MRC receiver operating on identically distributed and arbitrarily correlated Nakagami-m fading channels is equal to

$$\mathcal{M}_\gamma(s) = \prod_{b=1}^{B} \left(1 - \frac{s\overline{\gamma}_b}{m}\lambda_b\right)^{-m}, \tag{1}$$

where s is the transform variable, and $\{\lambda_b\}_{b=1}^{B}$ denotes the set of eigenvalues associated with a channel power correlation matrix $\mathbf{C}$. Applying Proposition 3 in [10] to this MGF, the SER performance of the fixed rate SIMO system (at high CSNR) is characterized by

$$G_d = Bm, \tag{2}$$

and

$$G_c = k\left(\frac{2^{Bm-1}v\Gamma(Bm+\frac{1}{2})}{\sqrt{\pi}\Gamma(Bm+1)}\right)^{-1/Bm}, \tag{3}$$

where $v = [\det(\mathbf{C})]^{-m} \cdot m^{Bm}$, and k is a fixed code-dependent positive constant [10]. When the exact PDF in [11] is approximated by a gamma distribution $\gamma \sim \mathcal{G}(\psi, \theta)$, the MGF is equal to

$$\mathcal{M}_\gamma(s) = \frac{1}{(1 - s\theta)^\psi}, \tag{4}$$

in which case the SER performance of the fixed rate SIMO system (at high CSNR) is characterized by

$$G_d = \psi, \tag{5}$$

and

$$G_c = k\left(\frac{2^{\psi-1}v\Gamma(\psi+\frac{1}{2})}{\sqrt{\pi}\Gamma(\psi+1)}\right)^{-1/\psi}, \tag{6}$$

where $v = (B/\psi)^{-\psi}$.

In Figure 2, G_d (top panel) and G_c (bottom panel) are depicted as functions of ρ_s for BPSK[3] transmission on Rayleigh fading channels ($m = 1$ and $k = 2$ [10]). Since G_d for the exact PDF is fixed and equal to B, the top panel presents G_d based on the approximate PDF only. It is observed that the error rate curve quickly deviates from the true slope as ρ_s increases. Hence, SER results based on the approximate PDF are likely to be in error at high CSNR compared to that obtained with the exact PDF. In the bottom panel, G_c is visualized for $B = 4$ for both a constant and an exponential correlation model. The results establish the amount of horizontal displacement (in dB) of the error rate curve (at high CSNR) relative to a benchmark curve $\overline{\gamma}^{-G_d}$ ($G_c = 0$ dB) as a function of ρ_s. As an example, it is observed that G_c based on both the exact and the approximate PDF and an exponential correlation model is approximately equal to 0 dB at $\rho_s = 0.7$. The impact of a reduced correlation level can then be quantified by observing that G_c increases as ρ_s decreases. This amounts to a left-shifted displacement of the error rate curve, i.e. a performance improvement. The

[3]Binary phase-shift keying.

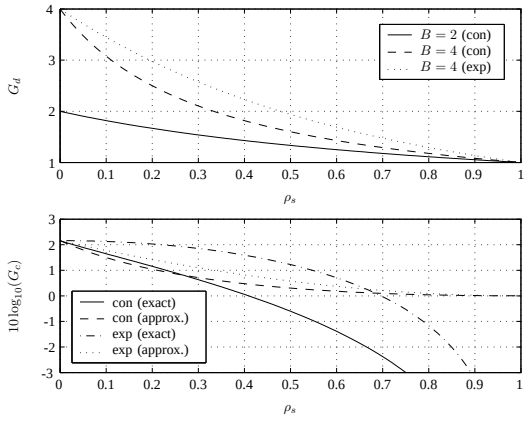


Fig. 2. Diversity and coding gain realized at high CSNR for a system operating on identically distributed spatially correlated Rayleigh fading channels, using BPSK transmission only. The abbreviations con and exp in the legends of both subfigures are related to results obtained with a constant and exponential correlation model, respectively. Top panel: G_d in (5) obtained with the approximate PDF is depicted. It should be related to G_d in (2), obtained with the exact PDF, in which case $G_d = B$. Bottom panel: Expressions for G_c in (3) and (6) are depicted for $B = 4$.

TABLE I

EXPRESSIONS FOR ψ AND θ FOR CONSTANT AND EXPONENTIAL CORRELATION MODELS

Correlation model	ψ	θ
Constant	$\frac{Bm}{1+\rho_s(B-1)}$	$\frac{\overline{\gamma}_b}{m}(1+\rho_s(B-1))$
Exponential	$\frac{Bm}{1+\frac{2\rho_s}{1-\rho_s}\left(1-\frac{1-\rho_s^B}{B(1-\rho_s)}\right)}$	$\frac{\overline{\gamma}_b}{m}\left(1+\frac{2\rho_s}{1-\rho_s}\left(1-\frac{1-\rho_s^B}{B(1-\rho_s)}\right)\right)$

amount of displacement obtained with the exact PDF is more rapid than that obtained with approximate PDF. Combining this result with G_d in the top panel, the error rate curve using the exact PDF will retain its slope during the displacement, whereas the error rate curve based on the approximate PDF will gradually increase its slope until it reaches B ($\rho_s = 0$). An increase beyond $\rho_s = 0.7$ amounts to a performance degradation.

In Section VII, $\rho_s = 0.2$ and $\rho_s = 0.7$ are selected for numerical analysis. This is due to the relatively good match observed for $B = 4$ and constant correlation at $\rho_s = 0.2$, and similarly for $B = 4$ and an exponential correlation of $\rho_s = 0.7$. In these cases, the approximate PDF realizes the same displacement of the error rate curve as the exact PDF.

V. CORRELATION BETWEEN TRUE AND PREDICTED CSNR

The correlation ρ between γ and $\hat{\gamma}$ is an important parameter affecting the BER performance of the ACM system. For a constant correlation model, ρ may be expressed as

$$\rho = \frac{B(\mathcal{E}\{\hat{\alpha}_b^2\alpha_b^2\} + (B-1)\mathcal{E}\{\hat{\alpha}_b^2\alpha_a^2\}) - (B\Omega)^2 r}{(B\Omega)^2 r} \cdot \psi. \quad (7)$$

In contrast to [6, Eq. (8)], ρ now involves correlation in both space and time, since α_a^2 is the instantaneous fading power on branch a, whereas $\hat{\alpha}_b^2$ is the instantaneous fading power on branch b, *predicted ahead in time* to compensate for the time delay on the feedback channel. The prediction horizon is assumed to be identical to the time delay on the feedback channel.

In this paper, spatial/temporal separability is assumed, i.e. the normalized cross correlation coefficient between complex fading amplitudes on different branches and at different lags is represented by a product of the individual spatial and temporal correlations.[4] As a result, it can be shown that (7) reduces to

$$\rho = \frac{|\mathbf{f}_\tau^{\mathrm{H}}\mathbf{r}_\tau|^2}{r}, \quad (8)$$

where $\mathbf{f}_\tau$ is the MAP-optimal predictor filter coefficient vector [6, Eq. (24)] (identical on each branch), and $\mathbf{r}_\tau$ is a normalized covariance vector [6, Eq. (25)], containing the covariance between the fading at the pilot symbol instants and the fading to be predicted at time instant $i+\tau$.[5] The result in (8) is in fact identical to the result for ρ obtained for spatially uncorrelated channels, and it holds for both a constant and an exponential correlation model. As such, all the results for ρ depicted in [6, Sec. VB] are equally valid for the results presented in this paper.

[4]According to [12], separable temporal and spatial correlations is adequate for gauging *average* system behavior.

[5]The superscript $(\cdot)^{\mathrm{H}}$ denotes the Hermitian transpose operator.

VI. ASE AND BER ANALYSIS

Closed-form expressions for the ASE and the average BER are derived in the same fashion as in [6, Sec. IV]. Hence, ASE $= \sum_{n=1}^{N} R_n P_n$, where $P_n = \int_{\gamma_n}^{\gamma_{n+1}} f_{\hat{\gamma}}(\hat{\gamma})d\hat{\gamma}$ is the probability of selecting code n, and $f_{\hat{\gamma}}(\hat{\gamma})$ is the (approximate) PDF of $\hat{\gamma}$ introduced in Section III. The average BER is obtained as

$$\overline{\mathrm{BER}} = \frac{\sum_{n=1}^{N} R_n \cdot \overline{\mathrm{BER}}_n}{\sum_{n=1}^{N} R_n \cdot P_n}, \quad (9)$$

where $\overline{\mathrm{BER}}_n$ is the average BER when code n is applied. It can be expressed as

$$\overline{\mathrm{BER}}_n = \int_{\gamma_n}^{\gamma_{n+1}} \int_0^{\infty} \mathrm{BER}_n(\gamma|\hat{\gamma}) f_{\gamma,\hat{\gamma}}(\gamma,\hat{\gamma}) d\gamma d\hat{\gamma}, \quad (10)$$

where $\mathrm{BER}_n(\gamma|\hat{\gamma})$ is the instantaneous BER experienced on an AWGN channel when code n is applied [6, Eq. (14)]. Furthermore, $f_{\gamma,\hat{\gamma}}(\gamma,\hat{\gamma})$ is the joint distribution of γ and $\hat{\gamma}$, which in this paper is identical to the (approximate) bivariate gamma distribution introduced in Section III.[6]

VII. NUMERICAL EXAMPLES

For comparison reasons, similar system parameters as in [6] are applied. The Jakes (temporal) fading spectrum is used, but the analytical framework does not place any constraints on the actual shape of the temporal autocorrelation sequence and corresponding Doppler spectrum. Parameters not directly tied to the codes, albeit dependent on the implementation, are the carrier frequency $f_c = 2$ GHz, bandwidth $W = 400$ kHz, and a terminal velocity of $v = 30$ m/s. The prediction filter length is $K = 1000$, the target BER is $\mathrm{BER}_0 = 10^{-4}$, and the pilot symbol spacing $L = 10$ (number of symbol periods between two successive pilot symbols).

In Figures 3 and 4, results for the average BER for $B = 4$ are presented as a function of $\overline{\gamma}_b$ and normalized feedback time delay.[7] In Figure 3, the result for uncorrelated channels is depicted, whereas in Figure 4, the result for exponentially correlated channels with $\rho_s = 0.7$ is depicted. Note that for a

[6]Note that in this paper, system performance is evaluated based on the switching thresholds $\{\gamma_n\}_{n=1}^N$, which are defined by assuming perfect knowledge of the true CSNR. The selection of a code however, is based on an estimated CSNR. The switching thresholds could have been adjusted to account for this fact, as reported in [13], [14]. However, the MAP-optimal predictor is negative biased, which means that the CNSR will tend to be underestimated. The bias will then not contribute to increase the BER, but it will reduce the ASE compared to an unbiased estimate.

[7]The time delay τ is assumed to be an integer number of pilot symbol intervals $\tau = iLT_s = jT_s$, where $j = iL$. The normalized time delay τ_{norm} is then equal to $\tau_{norm} = \tau/T_D = j \cdot f_D T_s$, where $T_D = 1/f_D$, f_D is the maximum Doppler frequency, and T_s is the duration of a single channel symbol.

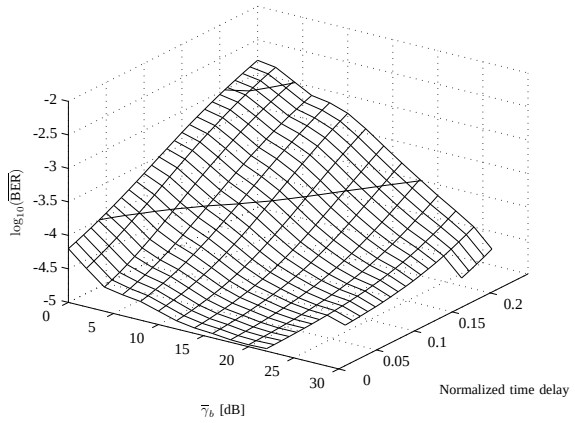


Fig. 3. Average BER as a function $\overline{\gamma}_b$ and normalized time delay on the feedback channel when $B = 4$ and the system operating on uncorrelated Rayleigh fading channels. The pilot symbol spacing $L = 10$, and the prediction filter length is $K = 1000$.

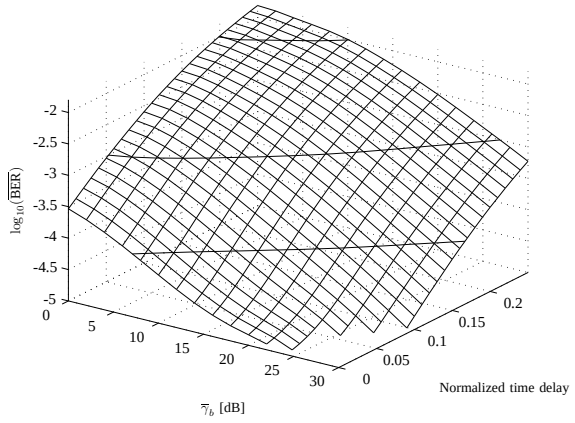


Fig. 4. Average BER as a function $\overline{\gamma}_b$ and normalized time delay on the feedback channel when $B = 4$ and the system is operating on exponentially correlated Rayleigh fading channels ($\rho_s = 0.7$). The pilot symbol spacing $L = 10$, and the prediction filter length is $K = 1000$.

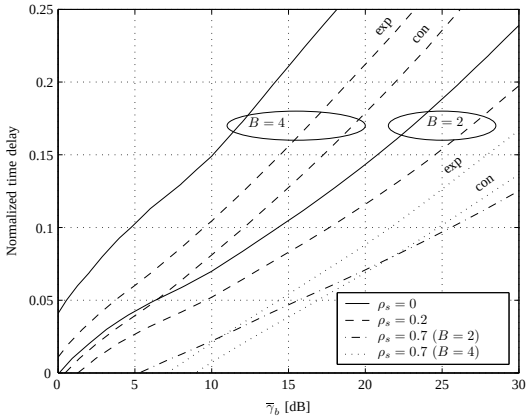


Fig. 5. Regions where the system performance is acceptable, plotted for $B = \{2, 4\}$, $L = 10$, $K = 1000$, and $\rho_s = \{0, 0.2, 0.7\}$. The curves indicate the largest delay that is allowed in order to achieve the BER requirements for a given average CSNR $\overline{\gamma}_b$. Thus, the performance is acceptable for each point specified by a CSNR/delay combination that is below and to the right of the curves.

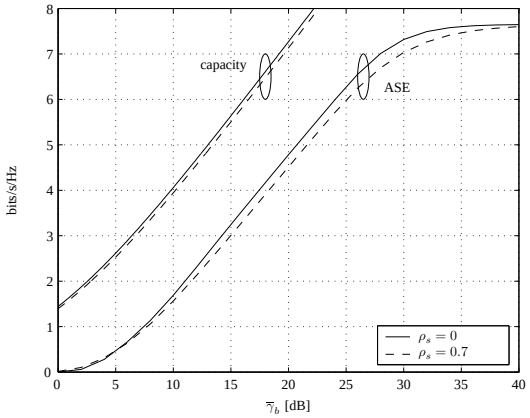


Fig. 6. Zero-delay ASE compared to the channel capacity (optimal rate adaptation with constant transmit power) [15, Sec. IV] for $B = 2$ and $\rho_s = \{0, 0.7\}$.

given target BER_0, the operation of the system is perceived as acceptable whenever the BER $< \text{BER}_0$. The shape of the BER surface is, therefore, not significant, except for the contour line at $\text{BER}_0 = 10^{-4}$. In Figure 5, several of such contour lines at $\text{BER}_0 = 10^{-4}$ have been plotted for $B \in \{2, 4\}$, $L = 10$, and $\rho_s \in \{0, 0.2, 0.7\}$. The curves indicate the largest time delay that is allowed in order to achieve the target $\text{BER}_0 = 10^{-4}$ for each given value of $\overline{\gamma}_b$, so performance is acceptable for any CSNR/delay combination below and to the right of the curves. It is observed that by predicting the channels independently, the presence of spatial correlation reduces the acceptable feedback delay. In particular, for $\overline{\gamma}_b = 10$ dB, $B = 2$, and $L = 10$, an acceptable feedback delay of 350 μs was obtained in [6]. For $\rho_s = 0.7$, the acceptable delay is reduced to 103 μs, i.e. approximately one third of the acceptable delay obtained with uncorrelated antennas.

When the system is operating at acceptable BER levels (below BER_0), ASE is the key performance measure. In Figure 6 ($B = 2$) and Figure 7 ($B = 4$), the zero-delay ASE realized for uncorrelated channels [6, Fig. 11] is compared to the corresponding ASE on correlated channels for $\rho_s = 0.7$. As a reference, results for the channel capacity on identically distributed and spatially correlated Rayleigh fading channels using optimal rate adaptation and constant transmit power are included [15, Sec. IV], and we see that the performance degradation for the capacity and the ASE due to spatial correlation is on the same small order. However, the ASE for correlated channels in Figures 6 and 7 are only valid for CSNR values where the target BER is achieved. Thus, it can be deduced from Figure 5 that the ASE curves for correlated channels in Figures 6 and 7 only are meaningful for $\overline{\gamma}_b > 5$ dB for $B = 2$ and $\overline{\gamma}_b > 7$ dB for $B = 4$.

For uncorrelated channels, it was observed in [6, Fig. 10] that the ASE is almost independent of the feedback time delay. Since the final result for ρ in (8) is unchanged from that obtained on uncorrelated channels, this trend is also observed for correlated channels. In Figure 8, this fact is illustrated by presenting the ASE in a three-dimensional graph as function of $\overline{\gamma}_b$ and normalized feedback time delay for $B = 2$ and

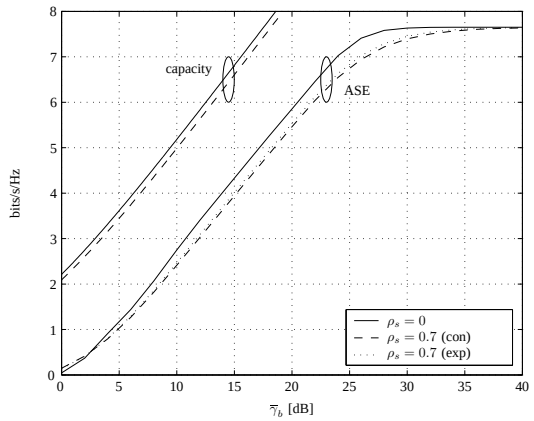


Fig. 7. Zero-delay ASE compared to the channel capacity (optimal rate adaptation with constant transmit power) [15, Sec. IV] for $B = 4$ and $\rho_s = \{0, 0.7\}$.

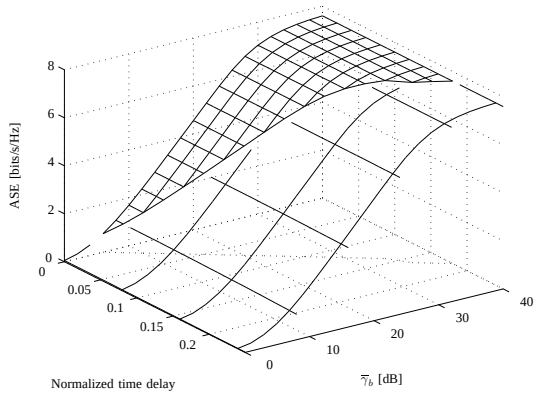


Fig. 8. ASE as a function of $\overline{\gamma}_b$ and normalized feedback time delay when $L = 10$, $B = 2$, and $\rho_s = 0.7$. The contour line divides the ASE into a relevant part where the BER constraints are fulfilled (to the left of the contour line) and an irrelevant part where the BER constraints are violated (to the right of the contour line). The prediction filter length is $K = 1000$.

$\rho_s = 0.7$. The contour line, which is identical to the one in Figure 5 with legend $\rho_s = 0.7$ $(B = 2)$, divides the ASE into a relevant part where the BER constraints are fulfilled (above the contour line (smaller grid)) and an irrelevant part where they are violated (below the contour line (larger grid)). Compared to a similar result for uncorrelated channels in [6, Fig. 10], the relevant part has been reduced due to spatial correlation between the antennas.

VIII. Conclusions

The impact of spatial correlation on ACM performance on identically distributed and spatially correlated Rayleigh fading channels has been investigated. It is observed that spatial correlation has a significant impact on the BER performance of an ACM system designed for spatially uncorrelated channels, by reducing the acceptable BER region where the system operates reliably with respect to average CSNR and permitted time delay on the feedback channel. To avoid this effect, the adaptation parameters must be re-designed to explicitly take spatial correlation into account, but this has not been a topic for study in this paper. When the system operates below the target BER_0 (acceptable region), the performance degradation in terms of ASE caused by spatial correlation is not large.

The results in this paper are based on two assumptions: (i) the exact PDF of the CSNR at the output of an MRC receiver can be approximated by a gamma distribution having identical first and second order moments to those of the exact PDF (ii) spatial/temporal separability is assumed, i.e. the normalized cross correlation between complex fading amplitudes on different branches is represented by a product of the individual spatial and temporal correlations. As a result, the temporal correlation between the true and predicted CSNR is unchanged from the case of uncorrelated channels reported in [6]. Using a more elaborate cross correlation function [16] may lead to different results.

References

[1] A. J. Goldsmith and S. -G. Chua, "Adaptive coded modulation for fading channels," *IEEE Transactions on Communications*, vol. 46, no. 5, pp. 595–602, May 1998.

[2] D. L. Goeckel, "Adaptive coding for time-varying channels using outdated fading estimates," *IEEE Transactions on Communications*, vol. 47, no. 6, pp. 844–855, June 1999.

[3] M. S. Alouini and A. J. Goldsmith, "Adaptive modulation over Nakagami fading channels," *Wireless Personal Communications*, vol. 13, pp. 119–143, May 2000.

[4] K. J. Hole, H. Holm, and G. E. Øien, "Adaptive multidimensional coded modulation on flat fading channels," *IEEE Journal on Selected Areas in Communications*, vol. 18, no. 7, pp. 1153–1158, July 2000.

[5] B. Holter, *Adaptive coded modulation in spatial and multiuser diversity systems*, Ph.D. thesis, Norwegian University of Science and Technology, June 2005 (available online at www.iet.ntnu.no/projects/beats/Documents/holter-thesis.pdf).

[6] G. E. Øien, H. Holm, and K. J. Hole, "Impact of channel prediction on adaptive coded modulation performance in Rayleigh fading," *IEEE Transactions on Vehicular Technology*, vol. 53, no. 3, pp. 758–769, May 2004.

[7] C. Mun, C. -H. Kang, and H. -K. Park, "Approximation of SNR statistics for MRC diversity systems in arbitrarily correlated Nakagami fading channels," *IEE Electronics Letters*, vol. 35, no. 4, pp. 266–267, February 1999.

[8] B. Holter and G. E. Øien, "On the amount of fading in MIMO diversity systems," *IEEE Transactions on Wireless Communications*, vol. 4, no. 5, pp. 2498–2507, September 2005.

[9] B. Holter and G. E. Øien, "Impact of spatial correlation on adaptive coded modulation performance in Rayleigh fading," *submitted to IEEE Transactions on Vehicular Technology*, February 2006 (available online at www.iet.ntnu.no/∼duong/publications/holter-vt-2005.pdf).

[10] Z. Wang and G. B. Giannakis, "A simple and general parameterization quantifying performance in fading channels," *IEEE Transactions on Communications*, vol. 51, no. 8, pp. 1389–1398, August 2003.

[11] M. -S. Alouini, A. Abdi, and M. Kaveh, "Sum of gamma variates and performance of wireless communication systems over Nakagami-fading channels," *IEEE Transactions on Vehicular Technology*, vol. 50, no. 6, pp. 1471–1479, November 2001.

[12] P. J. Smith and M. Shafi, "The impact of complexity in MIMO channel models," *in Proc. IEEE International Conference on Communications*, vol. 5, pp. 2924–2928, June 2004.

[13] D. V. Duong and G. E. Øien, "Adaptive trellis-coded modulation with imperfect channel state information at the receiver and transmitter," *in Proc. Nordic Radio Symposium*, August 2004.

[14] O. Jetlund, *Adaptive coded modulation: Design and simulation with realistic channel state information*, Ph.D. thesis, The Norwegian University of Science and Technology, April 2005 (available online at www.iet.ntnu.no/projects/beats/Documents/Jetlund_thesis.pdf).

[15] R. K. Mallik, M. Z. Win, J. W. Shao, M. -S. Alouini, and A. J. Goldsmith, "Channel capacity of adaptive transmission with maximal ratio combining in correlated Rayleigh fading," *IEEE Transactions on Wireless Communications*, vol. 3, no. 4, pp. 1124–1133, July 2004.

[16] A. Abdi and M. Kaveh, "A versatile spatio-temporal correlation function for mobile fading channels with non-isotropic scattering," *in Proc. 10th IEEE Workshop on Statistical Signal and Array Processing*, pp. 58–62, August 2000.